This is a preprint, the final version is subject to change, of the American Mineralogist (MSA)
Cite as Authors (Year) Title. American Mineralogist, in press.
(DOI will not work until issue is live.) DOI: http://dx.doi.org/10.2138/am.2014.4607

Revision 2

The two aluminum sites in the ^{27}Al MAS NMR spectrum of kaolinite : Accurate determination of isotropic chemical shifts and quadrupolar interaction parameters

Michaël Paris

Institut des Matériaux Jean Rouxel (IMN), Université de Nantes, CNRS. 2, rue de la Houssinière, BP 32229, 44322 Nantes Cedex 03, France.

ABSTRACT

The problem of resolving the two aluminum sites in the ^{27}Al NMR spectrum of kaolinite has been unsuccessfully addressed for thirty years. A few years ago, it was shown that the 2 sites cannot be spectrally separated even by the use of high magnetic fields. Nevertheless, it is still possible to determine the NMR parameters of both sites. In this article, we present an alternative approach. We show that, at low magnetic field (7 T), the individual spinning sideband lineshapes of the outer satellite transitions are sensitive enough to differentiate information coming from the two aluminum sites. Thus, the isotropic chemical shift δ, the quadrupolar constant C_Q and asymmetry parameter η_Q of each site can be obtained by accurately fitting the full ^{27}Al MAS spectrum acquired at low magnetic field. In return, this approach requires a carefully acquired and post-treated ^{27}Al spectrum. It is concluded that the two sets of parameters (δ=7.5 ppm, C_Q=3.4 MHz, η_Q=0.8) and (δ=8.0 ppm, C_Q=3.0 MHz, η_Q=0.9) represent the best and the unique solution overall. Moreover, the accuracy of these experimental values is independently and fully supported by first-principles calculations of the electric field gradient.

The approach presented in this article can be easily applied, not only to clays or aluminosilicate materials, but to any compounds where the NMR parameters of overlapping spectral lines have to be

determined. This can also be extended to sites of unequal multiplicity and to other nuclei. Moreover, this methodology can be useful in the characterization of small structural changes occurring partly at one particular site. Indeed, when the NMR parameters are barely modified, the spectral signatures due to both affected and unaffected sites may strongly overlap, making the spectral resonances broad and badly resolved. In such a case, determining the isotropic chemical shift and the quadrupolar coupling parameters may help to exceed the simple qualitative analysis of structural changes by offering the possibility of discriminating between structural models via the experimental data.

Keywords: Kaolinite, ^{27}Al MAS NMR, isotropic chemical shift, quadrupolar parameters, EFG calculations

INTRODUCTION

Kaolinite is an aluminosilicate used in a large variety of applications such as ceramics, building, paper or rubber materials. Kaolinite ($Al_2Si_2O_5(OH)_4$) has a 1:1 layered structure consisting of an octahedral aluminum hydroxide sheet and a tetrahedral silica sheet. The crystallographic structure determined by Bish (1993) is described in the conventional C1 space group with cell parameters of a=5.1535(3) Å, b=8.9419(5) Å, c=7.3906(4) Å, α=91.926(2)°, β=105.046(2)° and γ=89.797(2)°. Moreover, for both Si and Al atoms, there are two inequivalent crystallographic sites.

As a local technique, NMR is a powerful tool to gain information about the kaolinite structure and the modifications induced by thermal or chemical treatments. Indeed, determining the values of the parameters describing the NMR interactions experienced by the nuclei can provide insights on the polyhedra geometry (number of edges, angles) or connectivity leading to information on atom substitutions or deformations under treatment. Some hydraulic binder – kaolinite blends show structural modifications of two of the three interlayer hydroxyl groups. Similarly, exfoliation also modifies the structural configurations of the interlayer OH groups. Unfortunately, in kaolinite, these

groups can not be spectrally separated and characterized by ^{1}H NMR spectroscopy. ^{27}Al NMR may provide an alternative way if the corresponding parameters are precisely known. ^{27}Al is subject to the quadrupolar interaction resulting from the interaction between the quadrupole moment (Q) and the local Electric Field Gradient (EFG). This interaction is described by two parameters, the quadrupolar constant $C_Q=eV_{ZZ}Q/h$ and the asymmetry parameter $\eta_Q=(V_{YY}-V_{XX})/V_{ZZ}$ where V_{XX} ,V_{YY} and V_{ZZ} are the components of the electric field gradient expressed in its principal axis system (PAS) with $|V_{ZZ}|>|V_{XX}|>|V_{YY}|$. e is the electron charge and h Planck's constant. Note that only the absolute value of C_Q is accessible by experiment. In the case of ^{27}Al nuclei in aluminosilicate materials, the chemical shift anisotropy is generally small and can be neglected. Then, only the isotropic chemical shift δ and the quadrupolar coupling parameters are relevant.

The first ^{29}Si and ^{27}Al NMR spectra of kaolinite were acquired thirty years ago (Barron et al. 1983; Meinhold et al. 1985; Watanabe et al. 1987; Lambert et al. 1989). Although the existence of the two Si inequivalent sites in the ^{29}Si NMR spectrum was proved early (Barron et al. 1983), evidence for two octahedral ^{27}Al resonances is still controversial because the ^{27}Al NMR parameter values are expected to be close due to the two similar aluminum environments but also, in some cases, to the inadequate crystallinity of the kaolinite sample (Rocha 1999; Lee et al. 2003). To our knowledge, nine studies have reported so far values for C_Q, η_Q and δ. Among them, only two have reported values for both sites. All these values are gathered in the Table 1. As easily seen, some discrepancies exist.

The aim of this article is to determine, with a high degree of confidence and a high accuracy, the C_Q, η_Q and δ values of the two ^{27}Al sites of the kaolinite structure. First, the methodology used in this work will be presented. Then, the experimental values will be derived and their relevance will be discussed in light of first-principles calculations of EFG.

EXPERIMENTAL METHODS

Material

The sample of kaolinite with low-defects content (KGa-1b from Georgia, USA) was obtained from the Clay Minerals Society.

^{27}Al NMR spectroscopy

All experiments were conducted on Bruker Avance III 300 (7 T) and 500 MHz (11.75 T) spectrometers (^{27}Al Larmor frequencies of 78.2 MHz and 130.3 MHz, respectively) using 2.5 mm CP-MAS probes with a MAS frequency of 30 kHz and a repetition time of 1 s.

The ^{27}Al CT (Central Transition) MAS spectrum (11.75 T) was acquired with a $\pi/14$ excitation pulse and a radio-frequency (RF) field strength of 6 kHz.

The ^{27}Al Rotor-Synchronized acquisition (RSa) (Ashbrook and Wimperis 2005) spectra (11.75 T) were acquired with a $\pi/8$ excitation pulse length for a 120 kHz RF field. Such spectra are free from first-order quadrupolar interaction broadening. Inserting a π selective pulse prior to detection induced a Double-Quantum filtering allowing the first satellite transition only to be detected. The RF field of this soft pulse was 15 kHz.

Prior to acquisition of the full ^{27}Al MAS spectrum at 7 T, the magic angle of the coil was carefully adjusted by running a ^{87}Rb STMAS experiment (Gan 2000) on a $RbNO_3$ compound. The full ^{27}Al MAS spectrum was then acquired over a 1.25 MHz spectral width with ^{1}H decoupling during acquisition. The pulse excitation length was 0.5 µs for a 120 kHz RF field strength. The 14 first points of the f.i.d. (free induction decay) lost during dead time were reconstructed using the backward linear prediction algorithm implemented in the Bruker topspin 3.0 software. Then, the baseline was corrected. Finally, the spectrum was multiplied by a Lorentzian function (centered at 0 ppm with a full width at half-

height of 360 kHz) for taking into account the quality factor of the probe (~210 at 78 MHz).

Calculations

^{27}Al NMR simulations

All the NMR simulations have been done using the SIMPSON 3.1 package (Bak et al. 2000). All the free induction decays (f.i.d.) were simulated in accordance with the experimental conditions by considering the isotropic chemical shift and quadrupolar interaction to a second-order approximation as variable parameters only. The powder averaging was performed using 4180 crystallite orientations (zcw4180 powder averaging file in SIMPSON) and 40 γ angles. All the r.m.s.d. (root mean square deviation) values given in the text refer to SIMPSON output values. The line broadening adjustment during r.m.s.d. calculations corresponds to an exponential multiplication of the f.i.d.

DFT calculations

DFT calculations have been performed using the VASP (Vienna Ab initio Simulation Package) (Kresse and Furthmuller 1996) and WIEN2K (Blaha et al. 2012) packages with the PBE functional for exchange and correlation (Perdew et al. 1996). We used, as a starting guess, the structure determined by Bish (1993) for kaolinite and the structure determined by Saalfeld and Wedde (1974) for gibbsite. Prior to calculations of the EFG, the geometry optimization of the crystalline structures was carried out using the VASP code. Only the internal coordinates of the atoms were relaxed (i.e. the experimental cell parameters were kept). Optimized fractional atomic coordinates are given in Supplementary Material (Tables SM1 and SM2). Then, EFG's were calculated using both the WIEN2K package and the VASP package in which the EFG/PAW method (Petrilli et al. 1998) was recently implemented. Integration of the Brillouin-zone was done by using a 3x3x3 Monkhorst-Pack k-points grid (Monkhorst and Pack 1976) for kaolinite and a 4x4x4 k-points grid for gibbsite. In the VASP calculations, the

convergence of the EFG calculations was achieved by expanding the plane wave basis set to an energy cut-off of 675 eV and 625 eV for kaolinite and gibbsite, respectively. For the kaolinite structure, the Full-Potential Linearized Augmented Plane Wave calculations (FP-LAPW) using WIEN2K was done with RMT-K_{max}=5.0, RMT(Al)=1.57 a.u., RMT(Si)=1.36 a.u., RMT(O)=1.18 a.u. and RMT(H)=0.64 a.u. For the gibbsite structure, we used RMT-K_{max}=4.0, RMT(Al)=1.55 a.u., RMT(O)=1.19 a.u. and RMT(H)=0.64 a.u. Finally, C_Q was calculated taking Q=14.66 fm^2 (Harris et al. 2001).

Methodology

Many NMR approaches have been attempted for determining the NMR parameters of the two ^{27}Al sites in kaolinite, but separating these two very similar environments is challenging.

The ^{27}Al RSa spectrum (Figure 1A), acquired at 11.75 T, evidences the central transition (CT) and the inner (ST1 : ±3/2 ↔ ±1/2) and outer (ST2 : ±5/2 ↔ ±3/2) satellite transitions. Such a spectrum is not perturbed by the first-order quadrupolar interaction. Thus, the transitions only exhibit second-order quadrupolar lineshapes resulting, for the satellite transitions, from the sum of all their individual spinning sidebands. Remarkably, ST1 and ST2 are well separated. This is unambiguously confirmed by the spectrum acquired with the additional Double-Quantum filtering (Figure SM1A in Supplementary Material) exhibiting the ST1 transition only. Yet, even if they are separated, the two ^{27}Al sites can not be easily resolved in the satellite resonances of the spectrum. The sideband pattern of the satellite transitions (SST) of kaolinite has been previously described in the literature (Rocha and Pedrosa de Jesus 1994; Lee et al. 2003; Zhou et al. 2009). From the analysis of the SST obtained at 9.4 T, Rocha and Pedrosa de Jesus (1994) have shown the two ^{27}Al sites but were not able to derive the NMR parameter values. In contrast, the SST acquired at 14.1 T by Lee et al. (2003) was well simulated by a single ^{27}Al site. An explanation proposed by these authors is the lower crystallinity of their kaolinite sample compared to that used by Rocha and Pedrosa de Jesus (1994). More recently, Zhou et al. (2009)

have shown that, at moderate (11.7 T) or high (21.1 T) fields, there is no apparent evidence for two ^{27}Al sites in the individual spinning sidebands. Then, they concluded that the SATRAS approach (Skibsted et al. 1991; Jäger 1992) failed when resolving the two sites. Furthermore, they showed that the MQ-MAS approach (Frydman and Harwood 1995) failed too. Finally, the ^{27}Al CT spectrum (Figure 1B) shows that the ST2 transition is excited even with very low power pulse of 6 kHz radio-frequency strength. Comparison with the spectrum in Figure 1A shows that the shoulder at 10 ppm in the CT spectrum is at least partly due to the ST1 transition. This prevents highly accurate determination of NMR parameters from the spectral decomposition of such a spectrum.

The broadening due to the second-order quadrupolar interaction terms is proportional to the inverse of the static field. Thus, higher magnetic fields lead to narrower lines and better resolution. But, in the case of kaolinite where it is known that the two ^{27}Al sites present similar NMR parameters with moderate quadrupolar constants C_Q, the use of high magnetic field will smooth down the difference in lineshape of the two ^{27}Al sites, making them indistinguishable. At the opposite, the use of low field (7 T) will heighten the lineshape difference of the ST2 transition which is the most broadened and shifted by the second-order quadrupolar terms (Samoson 1985). In addition, low-field acquisition has also the advantage, in conjunction with a high MAS speed, to greatly reduce chemical shift anisotropy and dipolar contributions to the spectrum. Such a ^{27}Al spectrum, which can be considered as governed by the quadrupolar interaction and by the isotropic chemical shift only, is shown in Figure 2A. In the present article, we propose to extract the isotropic chemical shift δ, the quadrupolar constant C_Q and the quadrupolar asymmetry parameter η_Q of each site by accurately fitting the full ^{27}Al MAS spectrum, paying attention to the ST2 transition lineshapes. This clearly requires a spectrum of high quality i.e. with carefully conducted acquisition and post-treatment (see Experimental section for details).

The direct fitting of the full MAS spectrum requires the optimization of the NMR parameters (δ, C_Q,

η_Q) and the adjustment of the line broadening and amplitude for each site, taking into account the 1:1 intensity ratio constraint. This head-on approach is highly delicate since it may converge toward a local minimum. Hence, we propose an alternate approach where this unique fit with 6 NMR parameters is replaced by a collection of fits where only one amplitude and one line broadening are adjusted.

For this, we proceed in the following way. First, we consider two ^{27}Al sites (hereafter labelled as α and β) and set their NMR parameters (δ^α, $C_Q{}^\alpha$, $\eta_Q{}^\alpha$) and (δ^β, $C_Q{}^\beta$, $\eta_Q{}^\beta$). The two free induction decays (f.i.d.) are calculated and co-added, thus directly fulfilling the 1:1 intensity ratio condition. Then, amplitude and line broadening applied to the "sum f.i.d." are adjusted to obtain the best root mean square deviation (r.m.s.d.) between its Fourier transform and the experimental spectrum. Thus, the NMR parameters of the two ^{27}Al sites of kaolinite are simply determined by the set of (δ^α, $C_Q{}^\alpha$, $\eta_Q{}^\alpha$, δ^β, $C_Q{}^\beta$, $\eta_Q{}^\beta$) giving the lowest r.m.s.d. value. All f.i.d. and r.m.s.d calculations have been performed with the SIMPSON package. In accordance with previous work (Table 1) and preliminary calculations, the δ and C_Q values can be restrained to the 1.5-13.0 ppm and 2.5-4.5 MHz ranges, respectively. Moreover, the Double-Quantum filtered ^{27}Al RSa spectrum acquired at 130 MHz (Figure SM1A in Supplementary Material) shows that the ST1 resonance is a thin and symmetric line. This requires that, whatever the C_Q values involved, the ^{27}Al isotropic chemical shifts of the 2 sites cannot be separated by more than 5 ppm (i.e. $|\delta^\alpha - \delta^\beta| \leq 5$ ppm) without the loss of ST1 lineshape symmetry and broadening. In a practical way, calculations were split in many blocks within which the δ^α and δ^β (with $\delta^\alpha \leq \delta^\beta$) values are fixed and all the ($C_Q{}^\alpha$, $\eta_Q{}^\alpha$, $C_Q{}^\beta$, $\eta_Q{}^\beta$) choices are varied. This offers an easy way of implementing the $|\delta^\alpha - \delta^\beta| \leq 5$ ppm condition. Finally, for exploring the ranges of the parameter values, we have chosen steps of 0.5 ppm, 0.1 MHz and 0.1 for δ, C_Q ,and η_Q, respectively.

RESULTS AND DISCUSSION

Experimental results

1-site model

A constructive point a view for discussing the results obtained from the fitting of the full ^{27}Al MAS spectrum with two sites may come from the comparison with those obtained by considering only a single site. In this case, Figure 2B shows the best fit obtained using the dmfit software (Massiot et al. 2002). The corresponding NMR parameters are δ=8.4 ppm, C_Q=3.26 MHz and η_Q=0.76 (Table 2). The sideband pattern of the ST1 transition is well reproduced. Considering the overall spectrum, this represents a good fit of the experimental spectrum (r.m.s.d. = 2.62) even if close inspection of the spectrum (Inset in Figure 2) shows that spinning sideband lineshapes of the ST2 transition are less well described. This result is not surprising since the two Al sites in the crystallographic structure have very similar environments. Nevertheless, considering a fit with two aluminum sites in accordance with the crystallographic structure should improve the reproduction of the spinning sideband lineshapes of the ST2 transition. If not, this fit will lead to two aluminum sites having parameters equal to those of the 1-site model.

2-site model

Figure 3 shows the contour plot of the lowest r.m.s.d values obtained from the fit of the ^{27}Al MAS spectrum as a function of δ^α and δ^β. Clearly, this means that each point is only associated with the set of (C_Q^α, η_Q^α, C_Q^β, η_Q^β) values giving the lowest r.m.s.d. for this pair of isotropic chemical shifts. Note that to facilitate viewing, the plot was symmetrized with respect to the first diagonal as only the upper side has been calculated ($\delta^\alpha \leq \delta^\beta$). The contour plot exhibits only one minimum in the (δ^α, δ^β) space which is centered at 8 ppm for both dimensions. This unambiguously defines the isotropic chemical shifts of the two ^{27}Al sites. The three lowest points have r.m.s.d. values below 1.9 and are located at

8.0/8.0, 8.0/7.5 and 7.5/8.5 ppm, respectively. Table 2 gives the NMR parameters values associated with each of them. As the differences between these values do not exceed the steps chosen for screening the parameter ranges, they represent the same solution. Hence, we will now consider the values (δ^{α}=8.0 ppm, C_Q^{α}=3.0 MHz, η_Q^{α}=0.9) and (δ^{β}=7.5 ppm, C_Q^{β}=3.4 MHz, η_Q^{β}=0.8) representative for discussion.

Let us now discuss the relevance of the 4 C_Q^{α}, η_Q^{α}, C_Q^{β} and η_Q^{β} values giving the best r.m.s.d. Among all the possibilities screened with this given (δ^{α}, δ^{β}) pair, it is possible that some other quite different sets of values can lead to very low r.m.s.d. values too. In other words, many minima may exist in the (C_Q^{α}, η_Q^{α}, C_Q^{β}, η_Q^{β}) space. In order to explore this four-dimensional space, we used two-dimensional projections in which each point corresponds to the best r.m.s.d. value along the two other dimensions. Thus, a point of the (C_Q^{α}, η_Q^{α}) projection gives the best r.m.s.d. reachable for these C_Q^{α} and η_Q^{α} values, whatever the C_Q^{β} and η_Q^{β} values. Figures 4 and 5 show four two-dimensional projections in the (C_Q^{α}, η_Q^{α}), (C_Q^{β}, η_Q^{β}), (C_Q^{α}, C_Q^{β}) and (η_Q^{α}, η_Q^{β}) planes of the (C_Q^{α}, η_Q^{α}, C_Q^{β}, η_Q^{β}) space for the (δ^{α}=8.0 ppm, δ^{β}=7.5 ppm) case. Because of the small chemical shift difference between δ^{α} and δ^{β}, the two sites act similarly. This induces a splitting of the minimum in the (C_Q^{α}, η_Q^{α}) and (C_Q^{β}, η_Q^{β}) projections (Figure 4). For the (C_Q^{α}, C_Q^{β}) and (η_Q^{α}, η_Q^{β}) projections, in contrast, it manifests itself by a quasi symmetry with respect to the first diagonal of the plots (Figure 5). Apart from splitting, both (C_Q^{α}, η_Q^{α}) and (C_Q^{β}, η_Q^{β}) projections show only one minimum corresponding to the values reported in Table 2. Moreover, the (C_Q^{α}, C_Q^{β}) projection shows that the best C_Q^{β} value associated with the C_Q^{α}=3.0 MHz value is 3.4 MHz. In a similar way, the best η_Q^{β} value associated with the η_Q^{α}=0.9 value is 0.8. This means that the (C_Q^{α}, η_Q^{α}, C_Q^{β}, η_Q^{β}) space presents only one minimum. Consequently, the values reported in Table 2 represent a unique solution, i.e. the unique set of (C_Q^{α}, η_Q^{α}, C_Q^{β}, η_Q^{β}) values for the given pair of isotropic chemical shifts (δ^{α}=8.0 ppm, δ^{β}=7.5 ppm).

Analogous conclusions apply for the two other cases, (δ^{α}=8.0 ppm, δ^{β}=8.0 ppm) and (δ^{α}=7.5 ppm, δ^{β}=8.5 ppm), reported in Table 2. Their 4 corresponding projections can be found in Figure SM4 and Figure SM5 in Supplementary Material. The splitting and the quasi symmetry just mentioned above lead to minima spatially well separated from each other (Figures 4, 5, SM4 and SM5). This means that average values, as derived from the 1-site model, are not adequate to reproduce the spectrum since they lie between the two minima (i.e. in a region of higher r.m.s.d). Hence, the difference in C_Q values between the α and β components is significant. Therefore, the screening step can be considered as the error on the quadrupolar coupling parameter.

The spectrum corresponding to the 2-site model is shown in Figure 2C. As the quadrupolar interaction to a second-order approximation barely influences the ST1 transition, this latter is largely governed by first-order terms which are not sensitive enough to separate two spectral components of similar NMR parameters. Clearly, in our case, the differences between the 2-site (C_Q^{α}=3.0 MHz and C_Q^{β}=3.4 MHz) and the 1-site (C_Q=3.26 MHz) models lead to differences in the spinning sideband intensities as well as in the total width of the ST1 transition which are hard to discriminate. In contrast, the ST2 transition is 44/7 times more broadened by the second-order quadrupolar interaction terms than the ST1 transition is (Samoson 1985). Hence, spinning sidebands of the ST2 transition have characteristic second-order lineshapes and are much more sensitive to small differences in quadrupolar coupling parameters. Thus, in addition to the quantitative approach from r.m.s.d. values, a qualitative demonstration of the improvement obtained by the 2-site model over the 1-site model is given by the better reproduction of the individual spinning sideband lineshapes of the ST2 transition (Inset in Figure 2). Furthermore, the better rendering of the overall ST2 transition lineshape by the 2-site model is also supported by the comparison of the simulated ^{27}Al RSa spectra derived from the two models with the experimental spectrum obtained at 11.75 T (Figure SM6 in Supplementary Material), even if this latter

is affected by cumulative errors in the sum of the individual spinning sidebands.

Thus, the two sets (δ^{α}=8.0 ppm, C_Q^{α}=3.0 MHz, η_Q^{α}=0.9) and (δ^{β}=7.5 ppm, C_Q^{β}=3.4 MHz, η_Q^{β}=0.8) with a precision of 1.0 ppm, 0.1 MHz and 0.1 for δ, C_Q and η_Q, respectively are the best choice to reproduce the NMR spectrum. As expected (vide supra), the NMR parameter values obtained are close to those of the 1-site model which gives confidence in these values. Moreover, they are also similar to those proposed by Hayashi et al. (1992) and Rocha and Pedrosa de Jesus (1994) (Table 1). But, in addition to these authors, we have, for the first time, demonstrated the uniqueness of the spectral decomposition.

Calculations results

The spectral decomposition of the ^{27}Al MAS spectrum presented above is accurate and convincing but assumes that the experimental uncertainties related to the acquisition conditions as well as to the post-treatments are below the level of the fit description achieved. Even if the experimental spectrum was acquired by setting the magic angle through a STMAS experiment, very small missetting can occur and slightly affect the spinning sideband manifold. Similarly, the experimental spectrum was post-treated with the most possible care by taking into account the quality factor of the probe but phasing, linear backward prediction or baseline correction may also influence the spectrum. Even if expected to be small, how much these effects can affect the final spectrum is hard to understand. This means that the experimental NMR parameter values of the two sites of kaolinite must be validated independently. This can be efficiently achieved by first-principles calculations of the NMR parameters from the well known crystallographic structure of kaolinite.

Hereafter, the two aluminum sites of the kaolinite structure will be labeled Al1 and Al2 in accordance with Bish (1993) and optimized fractional atomic coordinates given in Supplementary

Material. In the structure determined by Bish (1993), the local geometries of the two aluminum octahedra are very similar. This is clearly evidenced by using the quadratic elongation λ and the bond angle variance σ^2 which are quantitative measures of the polyhedral distortion in bond lengths and angles (Robinson et al. 1971). Indeed, before geometry optimization, one has λ=1.0173(5) and σ^2=63°^{2} for both sites. The main effect of the geometry optimization is to shorten the Al-O bond length on the interlayer side and lengthen them on the silica sheet side. This latter effect is more pronounced for the Al1-O2 and Al2-O1 bonds where O1 and O2 are the Al-O-Si bridging oxygens (Figure 6). The six angles deviating significantly from 90° are also reported in Figure 6. All others are given in Supplementary Material (Table SM3). After the geometry optimization, the O2--Al1--X (X = O1, O-H1, O-H2 or O-H3) and O1--Al2--Y (Y = O2, O-H1, O-H2 or O-H3) bond angles are slightly lower (-2.8° and -2.4° on average for Al1 and Al2, respectively). Accordingly, the O-H4--Al1--X and O-H4--Al2--Y angles are higher. Thus, the two octahedral geometries are more distorted than before the geometry optimization. The quadratic elongation and bond angle variance for the two octahedra are λ(Al1)=1.0206, σ^2(Al1)=70°^{2}, λ(Al2)=1.0193 and σ^2(Al2)=66°^{2}. Therefore, the octahedral environment of the Al1 site appears also more distorted than that of Al2.

For periodic systems, both chemical shift and quadrupolar parameters (EFG calculations) can be obtained by first-principles calculations in the field of density functional theory (DFT) using projector augmented-waves (PAW) approach. Nevertheless, compared to EFG, chemical shift calculations (Pickard and Mauri 2001) are by far more complex and computationally demanding. Until now, the precision of isotropic chemical shift values is no better than few ppm (Gervais et al. 2004; Choi et al. 2009; Bonhomme et al. 2012). Even if it is often sufficient in numerous cases for line assignments, it is not precise enough here where the two ^{27}Al sites are expected to have isotropic chemical shift difference of the order of one ppm or less. Then, such calculations will not be discussed since they are

not able to test accurately the parameter values extracted from the ^{27}Al MAS spectrum.

The EFG calculations on the ^{27}Al sites of kaolinite were based on the structure determined by Bish (1993) after optimization of the internal positions of the atoms in the unit cell. The C_Q and η_Q NMR parameters derived from the calculations using both the VASP and WIEN2K codes are reported in Table 3. Our experimental and calculated values are in good agreement. The η_Q values are well reproduced and the experimental C_Q values are 0.4 MHz lower than the calculated values. This difference is within the precision of the calculations of the ^{27}Al quadrupolar constants in aluminosilicates generally reported to be less than 0.5 MHz (Rocquefelte et al. 2007; Vyalikh et al. 2010). Even if this supports our experimental approach, strong conclusions on the accuracy of the experimental data can not be easily drawn because the difference between experimental and calculated C_Q values equals the difference in C_Q values between the two sites.

A way to circumvent this difficulty is to use a reference compound to test the reliability of our EFG calculations. This compound should present a structure as similar as possible to kaolinite and its ^{27}Al quadrupolar constants should be known accurately. For kaolinite, a good reference compound is gibbsite, an aluminum hydroxide ($Al(OH)_3$). Its crystallographic structure was determined by Saalfeld and Wedde (1974) and consists of layered octahedral aluminum hydroxide sheets. They are structurally very similar to the sheets of $Al_2(OH)_4$ octahedra found in the kaolinite structure and also have two crystallographic aluminum sites. But, in contrast to kaolinite, these latter have very different C_Q and η_Q values which have been accurately and unambiguously measured from a ^{27}Al CT MAS spectrum (Vyalikh et al. 2010). Thus, we have performed EFG calculations on the gibbsite structure with exactly the same approach as used for kaolinite. The experimental (Vyalikh et al. 2010) and our calculated C_Q and η_Q values are reported in Table 3. Similar to our results for kaolinite, the η_Q values are well reproduced but the experimental C_Q values are lower than those calculated by ~0.4 MHz. Previous EFG

calculations on gibbsite (Vyalikh et al. 2010) obtained with the CASTEP code show exactly the same trend i.e. the experimental values are lower by 0.5 MHz than the calculated ones.

Accurate calculations of EFG's need a good description of the core electrons of the aluminum atoms. In contrast to the all-electron FP-LAPW approach of the WIEN2K code, the VASP and CASTEP codes use a pseudo-potential formalism and the electronic core states are then reconstructed using the PAW method. The very good agreement between these two approaches shows that the EFG calculation is not the origin of the 0.4 MHz shift observed. The most probable explanation is an insufficient description of the hydrogen bonds in the interlayer due to the DFT, at the PBE level, which is known to inadequately describe weak interactions such as hydrogen bonds or van der Waals interactions. Then, the shift on C_Q values has to be related to the layered nature of the compound structures. This can explain why its value (~ 0.4 MHz) is the same whatever the aluminum sites, even for those having very different C_Q values as for gibbsite. This shows that the difference in C_Q values between the two aluminum sites of kaolinite is reproduced as well as for gibbsite. Consequently, these first-principles calculations of quadrupolar coupling parameters support our experimental values extracted from the ^{27}Al MAS spectrum and show that the experimental uncertainties related to the acquisition and post-treatment conditions are below the level of the fit description achieved. Furthermore, the two components, α and β, of the 2-site model can be attributed to the two crystallographic sites Al2 and Al1, respectively. Thus, as expected, the lowest C_Q value is associated with the less distorted site Al2 (λ(Al2)<λ(Al1)).

IMPLICATIONS

The methodology presented in this article succeeded in determining the isotropic chemical shift δ, the quadrupolar constant C_Q and the asymmetry parameter η_Q of the two very similar aluminum

environments of the kaolinite structure. This approach, requiring only a low magnetic field spectrometer, can be efficiently applied to other highly crystalline materials. Those include not only clays or aluminosilicate materials but any compounds whose spectra exhibit lines with very similar NMR parameters. The methodology can be adapted to sites of unequal multiplicity and to other nuclei, even if spin I=5/2 nuclei appear the most suitable regarding the broadening and shift (including sign) factors of the satellite transitions induced by the second-order quadrupolar interaction terms.

In future, the most useful application of this approach may be the characterization of small structural changes occurring partly at one particular site (initially spectrally well resolved). Indeed, when the NMR parameters are barely modified, the spectral signatures due to both affected and unaffected sites may strongly overlap and result in broadened and badly resolved spectral resonances. In such a case, determining the isotropic chemical shift and the quadrupolar coupling parameters may help to exceed the simple qualitative analysis of structural changes by offering the possibility of discriminating between structural models via the experimental data. Modifications in local environments can be induced, for example, by cation exchange, by cation substitution, by grafting molecules, by modification of the hydrogen bond network in some layered compounds... and potentially, by all processes that maintain the compound in a crystalline state and that do not introduce extra broadening of the spectrum (e.g. paramagnetic broadening). These kind of modifications are widely applied, for example, to the hydrotalcite-like layered double hydroxides (LDHs) compounds which are intensively studied for their use in a large range of applications such as drug delivery, catalysts, water treatment or flame-retardants.

ACKNOWLEDGEMENTS

The author would like to thank Dr. F. Boucher, Dr. J. Cody and Dr. C. Ewels for carefully reading the manuscript and the anonymous reviewers for their constructive comments.

REFERENCES CITED

Ashbrook, S.E., McManus, J., MacKenzie, K.J.D. and Wimperis, S. (2000) Multiple-Quantum and Cross-Polarized ^{27}Al MAS NMR of Mechanically Treated Mixtures of Kaolinite and Gibbsite. Journal of Physical Chemistry B, 104, 6408-6416.

Ashbrook, S.E. and Wimperis, S. (2005) Rotor-synchronized acquisition of quadrupolar satellite-transition NMR spectra: practical aspects and double-quantum filtration. Journal of Magnetic Resonance, 177, 44-55.

Bak, M., Rasmussen, J.T. and Nielsen, N.C. (2000) SIMPSON: A General Simulation Program for Solid-State NMR Spectroscopy. Journal of Magnetic Resonance, 147, 296-330.

Barron, P.F., Frost, R.L., Skjemstad, J.O. and Koppi, A.J. (1983) Detection of two silicon environments in kaolins by solid-state ^{29}Si NMR. Nature, 302, 49-50.

Bish, D.L. (1993) Rietveld refinement of the kaolinite structure at 1.5 K. Clays and Clay Minerals, 41, 738-744.

Blaha, P., Schwarz, K., Madsen, G.K.H, Kvasnicka, D. and Luitz, J. (2012) WIEN2k An Augmented PlaneWave + Local Orbitals Program for Calculating Crystal Properties. ISBN 3-9501031-1-2

Bonhomme, C., Gervais, C., Babonneau, F., Coelho, C., Pourpoint, F., Azais, T., Ashbrook, S.E., Griffin, J.M., Yates, J.R., Mauri, F. and Pickard, C.J. (2012) First-Principles Calculation of NMR

Parameters Using the Gauge Including Projector Augmented Wave Method: A Chemist's Point of View. Chemical Reviews, 112, 5733-5779.

Choi, M., Matsunaga, K., Oba, F. and Tanaka, I. (2009) ^{27}Al NMR Chemical Shifts in Oxide Crystals: A First-Principles Study. Journal of Physical Chemistry C, 113, 3869-3873.

Crosson, G.S., Choi, S.Y., Chorover, J., Amistadi, M.K., O'Day, P.A. and Mueller, K.T. (2006) Solid-state NMR Identification and Quantification of Newly Formed Aluminosilicate Phases in Weathered Kaolinite Systems. Journal of Physical Chemistry B, 110, 723-732.

Frydman, L. and Harwood, J.S. (1995) Isotropic Spectra of Half-Integer Quadrupolar Spins from Bidimensional Magic-Angle-Spinning NMR. Journal of the American Chemical Society, 117, 5367-5368.

Gan, Z. (2000) Isotropic NMR Spectra of Half-Integer Quadrupolar Nuclei Using Satellite Transitions and Magic-Angle spinning. Journal of the American Chemical Society, 122, 3242-3243.

Gervais, C., Profeta, M., Babonneau, F., Pickard, C.J. and Mauri, F. (2004) Ab Initio Calculations of NMR Parameters of Highly Coordinated Oxygen Sites in Aluminosilicates. Journal of Physical Chemistry B, 108, 13249-13253.

Harris, R.K., Becker, E.D., De Menezes, S.M.C., Goodfellow, R. and Granger, P. (2001) NMR nomenclature. Nuclear spin properties and conventions for chemical shifts - (IUPAC recommendations 2001). Pure and Applied Chemistry, 73, 1795-1818.

Hayashi, S., Ueda, T., Hayamizu, K. and Akiba, E. (1992) NMR Study of Kaolinite .1. ^{29}Si, ^{27}Al and ^{1}H Spectra. Journal of Physical Chemistry, 96, 10922-10928.

Jäger, C. (1992) How to Get More from ^{27}Al MAS NMR by High-Speed Satellite-Transition Spectroscopy. Journal of Magnetic Resonance, 99, 353-362.

Kresse, G. and Furthmuller, J. (1996) Efficient iterative schemes for ab initio total-energy calculations using a plane-wave basis set. Physical Review B, 54, 11169-11186.

Krøyer, H., Lindgreen, H., Jakobsen, H.J. and Skibsted, J. (2003) Hydration of Portland cement in the presence of clay minerals studied by ^{29}Si and ^{27}Al MAS NMR spectroscopy. Advances in Cement Research, 15, 103-112.

Lambert, J.F., Millman, W.S. and Fripiat, J. J. (1989) Revisiting Kaolinite Dehydroxylation: a ^{29}Si and ^{27}Al MAS NMR Study. Journal of the American Chemical Society, 111, 3517-3522.

Lee, S.K., Stebbins, J.F., Weiss, C.A. and Kirkpatrick, R.J. (2003) ^{17}O and ^{27}Al MAS and 3QMAS NMR Study of Synthetic and Natural Layer Silicates. Chemistry of Materials, 15, 2605-2613.

Massiot, D., Fayon, F., Capron, M., King, I., Le Calve, S., Alonso, B., Durand, J.O., Bujoli, B., Gan, Z. H. and Hoatson, G. (2002) Modelling one- and two-dimensional solid-state NMR spectra. Magnetic Resonance in Chemistry, 40, 70-76.

Meinhold, R.H., MacKenzie, K.J.D., and Brown, I.W.M. (1985) Thermal reactions of kaolinite studied by solid state 27-Al and 29-Si NMR. Journal of Materials Science Letters, 4, 163-166.

Monkhorst, H.J. and Pack, J.D. (1976) Special points for Brillouin-zone integrations. Physical Review B, 13, 5188-5192.

Newman, R.H., Childs, C.W. and Churchman, G.J. (1994). Aluminum coordination and structural disorder in halloysite and kaolinite by ^{27}Al NMR spectroscopy. Clay Minerals, 29, 305-312.

Perdew, J.P., Burke, K. and Ernzerhof, M. (1996) Generalized Gradient Approximation Made Simple. Physical Review Letters, 77, 3865-3868.

Petrilli, H.M., Blöchl, P.E. Blaha, P. and Schwarz, K. (1998) Electric-field-gradient calculations using the projector augmented wave method. Physical Review B, **57**, 14690-14697.

Pickard, C.J. and Mauri, F. (2001) All-electron magnetic response with pseudopotentials: NMR chemical shifts. Physical Review B, 63, 245101.

Robinson, K., Gibbs, G.V. and Ribbe, P.H. (1971) Quadratic Elongation: A Quantitative Measure of Distortion in Coordination Polyhedra. Science, 172, 567-570.

Rocha, J. and Pedrosa De Jesus, J.D. (1994) ^{27}Al Satellite Transition MAS-NMR Spectroscopy of Kaolinite. Clay Minerals, 29, 287-291.

Rocha, J. (1999) Single- and Triple-Quantum ^{27}Al MAS NMR Study of the Thermal Transformation of Kaolinite. Journal of the Physical Chemistry B, 103, 9801-9804.

Rocquefelte, X., Clabau, F., Paris, M., Deniard, P., Le Mercier, T., Jobic, S. and Whangbo, M.H. (2007) Resolving the Aluminum Ordering in Aluminosilicates by a Combined Experimental/Theoretical Study of ^{27}Al Electric Field Gradients. Inorganic Chemistry, 46, 5456-5458.

Saalfeld, H. and Wedde, M. (1974) Refinement of crystal structure of gibbsite, $Al(OH)_3$. Zeitschrift für Kristallographie, 139, 129-135.

Samoson, A. (1985) Satellite transition high-resolution NMR of quadrupolar nuclei in powders. Chemical Physics Letters, 119, 29-32.

Shulepov, Y., Litovchenko, A., Melnikov, A., Proshko, V. and Kulik, V. (1983) The Effects of Quadrupole Splitting of the Central ^{27}Al NMR Line in Polycrystalline Kaolinite. Journal of Magnetic Resonance, 53, 178-186.

Skibsted, J., Nielsen, N.C., Bildsøe, H. and Jakobsen, H.J. (1991) Satellite Transitions in MAS NMR Spectra of Quadrupolar Nuclei. Journal of Magnetic Resonance, 95, 88-117.

Vyalikh, A., Zesewitz, K. and Scheler, U. (2010) Hydrogen bonds and local symmetry in the crystal structure of gibbsite. Magnetic Resonance in Chemistry, 48, 877-881.

Watanabe, T., Shimizu, H., Nagasawa, K., Masuda, A. and Saito, H. (1987) ^{29}Si- and ^{27}Al-MAS/NMR

study of the thermal transformations of kaolinite. Clay Minerals, 22, 37-48.

Zhou, B., Sherriff, B.L. and Wang, T. (2009) ^{27}Al NMR spectroscopy at multiple magnetic fields and ab initio quantum modeling for kaolinite. American Mineralogist, 94, 865-871.

Figure captions

Figure 1. ^{27}Al Rotor-Synchronized acquisition (A) and Central Transition (B) MAS (30 kHz) spectra (11.75 T) of kaolinite KGa-1b. The central transition (CT), inner (ST1) and outer (ST2) satellite transitions are labeled.

Figure 2. ^{27}Al full MAS (30 kHz) spectrum (7 T) of kaolinite KGa-1b (A). Simulated spectra using the parameter values from the 1-site model (δ=8.4 ppm, C_Q=3.26 MHz and η_Q=0.76) (B), from the 2-site model (δ^α=8.0 ppm, $C_Q{}^\alpha$=3.0 MHz, $\eta_Q{}^\alpha$=0.9 and δ^β=7.5 ppm, $C_Q{}^\beta$=3.4 MHz, $\eta_Q{}^\beta$=0.8) (C). Individual lines for the site α (D) and β (E) of the spectrum C.

Figure 3. Contour map of the lowest r.m.s.d. obtained from the fit of the ^{27}Al MAS spectrum of kaolinite KGa-1b (Figure 2A) as a function of the isotropic chemical shifts δ^α and δ^β. Enlarged color map is available in Figure SM2 in Supplementary Material.

Figure 4. Lowest r.m.s.d. contour maps of the ($C_Q{}^\alpha$, $\eta_Q{}^\alpha$) (upper) and ($C_Q{}^\beta$, $\eta_Q{}^\beta$) (lower) projections of the ($C_Q{}^\alpha$, $\eta_Q{}^\alpha$, $C_Q{}^\beta$, $\eta_Q{}^\beta$) space for δ^α=8.0 ppm and δ^β=7.5 ppm. Enlarged color maps are available in Figure SM3 in Supplementary Material.

Figure 5. Lowest r.m.s.d. contour maps of the ($C_Q{}^\alpha$, $C_Q{}^\beta$) (upper) and ($\eta_Q{}^\alpha$, $\eta_Q{}^\beta$) (lower) projections of the ($C_Q{}^\alpha$, $\eta_Q{}^\alpha$, $C_Q{}^\beta$, $\eta_Q{}^\beta$) space for δ^α=8.0 ppm and δ^β=7.5 ppm. Enlarged color maps are available in Figure SM3 in Supplementary Material.

Figure 6. Local geometries for the two octahedral aluminum sites Al1 (left) and Al2 (right) of kaolinite after geometry optimization carried out using the VASP package. All optimized fractional atomic coordinates are available in Table SM1 in Supplementary Material. Distances are given in Å.

Table captions

Table 1. ^{27}Al isotropic chemical shift δ, quadrupolar constant C_Q and asymmetry parameter η_Q values reported in the literature for the two aluminum sites of kaolinite (or mean values if the two sites were not resolved). Note: [a] corresponds to the quadrupolar product $C_Q(1+\eta_Q^2/3)^{1/2}$.

Table 2. ^{27}Al isotropic chemical shift δ, quadrupolar constant C_Q and asymmetry parameter η_Q values for the 1-site model and for the three points of the 2-site model having the lowest r.m.s.d. in Figure 3 (see text for details).

Table 3. Experimental and calculated values of the quadrupolar constant C_Q (MHz) and asymmetry parameter η_Q with calculated Electric Field Gradient eigenvalues, V_{ZZ}, V_{YY} and V_{XX} (10^{21} V/m^2), for kaolinite and gibbsite structures. Note that only the absolute value of C_Q is accessible by experiment. Notes: [a] $C_Q=eV_{ZZ}Q/h$, $\eta_Q=(V_{YY}-V_{XX})/V_{ZZ}$ with $|V_{ZZ}|>|V_{XX}|>|V_{YY}|$. Q=14.66 fm^2 , [b] $\pm$ 0.1 MHz, [c] $\pm$ 0.1, [d] Experimental values from Vyalikh et al. (2010).

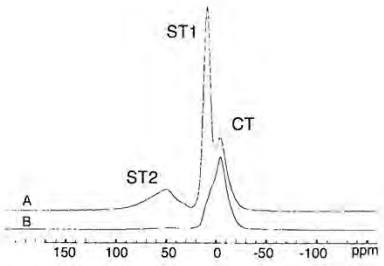

Figure 1.

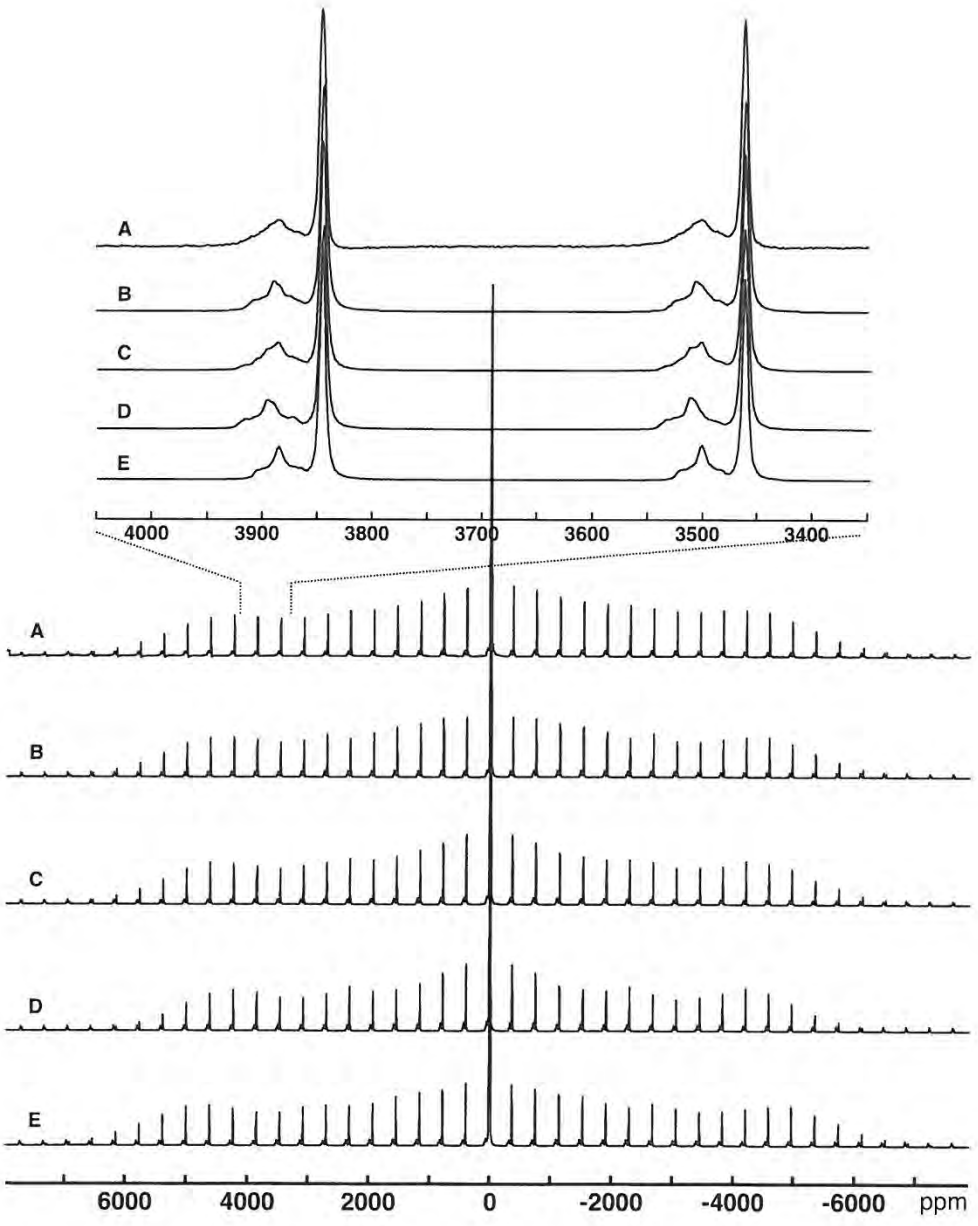
A
B
C
D
E
4000
3900
3800
3700
3600
3500
3400
A
B
C
D
E
6000
4000
2000
0
-2000
-4000
-6000
ppm

Figure 2.

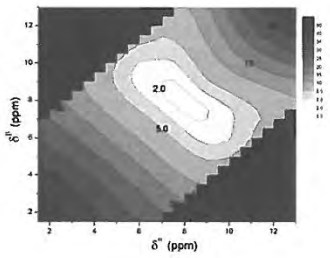

Figure 3.

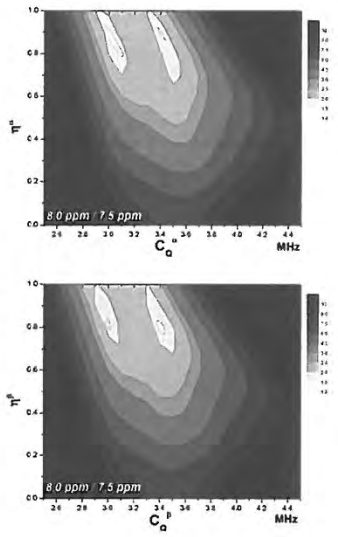

Figure 4.

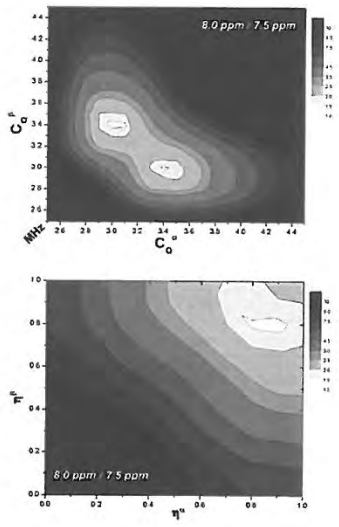

Figure 5.

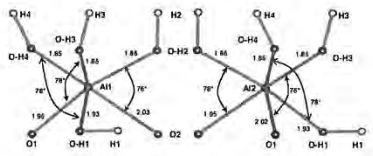
H4
H3
H2
O-H3
O-H4
O-H2
1.85
1.86
Al1
79°
76°
1.95
1.93
2.03
O1
O-H1
H1
O2
H4
H3
O-H4
O-H3
1.86
1.85
Al2
78°
1.95
2.02
1.93
O1
O-H1
H1

Figure 6.

	δ^{α} (ppm)	δ^{β} (ppm)	C_Q^{α} (MHz)	η_Q^{α}	C_Q^{β} (MHz)	η_Q^{β}
2-site values						
Hayashi et al. 1992	7.5	7.5	3.36	0.55	2.88	1.00
Rocha et al. 1994	8.9	7.8	3.53	0.67	2.89	0.97
Crosson et al. 2006	8.6	8.3	3.23[a]		1.84[a]	

Mean values	δ (ppm)	C_Q (MHz)	η_Q
Shulepov et al. 1983	-	3.12	0.95
Newman et al. 1994	10	3.4	0.7
Ashbrook et al. 2000	7	3.6[a]	
Krøyer et al. 2003	7.3	3.4	0.62
Lee et al. 2003	8.1	3.1	0.95
Zhou et al. 2009	6.25	2.6	0.75

Table 1.

	δ^{α} (ppm)	δ^{β} (ppm)	$C_Q{}^{\alpha}$ (MHz)	$C_Q{}^{\beta}$ (MHz)	$\eta_Q{}^{\alpha}$	$\eta_Q{}^{\beta}$	r.m.s.d.
2-site model	8.0	8.0	3.1	3.4	0.8	0.8	1.86
2-site model	8.0	7.5	3.0	3.4	0.9	0.8	1.87
2-site model	7.5	8.5	3.0	3.5	0.9	0.7	1.90
1-site model	8.4		3.26		0.76		2.62

Table 2.

		Measured		Calculated [a]					
		C_Q [b]	η_Q [c]	C_Q	η_Q		V_{ZZ}	V_{YY}	V_{XX}
Kaolinite	Site Al1	3.4	0.8	-3.76	0.69	*VASP*	-1.05943	0.16468	0.89474
				-3.85	0.66	*WIEN2K*	-1.08603	0.18205	0.90399
	Site Al2	3.0	0.9	-3.31	0.97	*VASP*	-0.93289	0.01391	0.91899
				-3.42	0.94	*WIEN2K*	-0.96396	0.02890	0.93506
Gibbsite [d]	Site #1	4.6	0.4	-4.96	0.35	*VASP*	-1.39902	0.45167	0.94735
				-4.74	0.35	*WIEN2K*	-1.33756	0.43199	0.90557
	Site #2	2.2	0.7	2.65	0.65	*VASP*	0.74823	-0.13073	-0.61750
				2.61	0.71	*WIEN2K*	0.73616	-0.10811	-0.62805

Table 3.